Note of Fast Runner

Ken

June, 2018*

1 About systems and methods

1.1 Requirements - system

- List of assumptions
- Capture the required parameters (i.e. how to normalize the systems)
  - Resonance
  - Nonlinear elastic components
    - a set of linear components for multiple modes?
-

1.2 Requirements - method

- Applicable to complex system (e.g. for the designed mechanism)
- Nondimensionlization (so that it can be used for robots with different scales)
- Stability analysis
- Robustness

1.3 Remarks

- Impact does not cause velocity change on runner with massless leg!
- In SCS, to simulate massless leg, it is better to use only one body, and manipulate the relation between the contact point and the body in controller instead.

1.4 ToDo

- Rearrange/updating references for fastRunner
- Check if the foot is sliding
- Check optimization tools ihmc have
  - parameter optimization tool using Gradient Decent or GA
- Ask Cris about the parameter range/selection

*Last update: June 27, 2018

1.5 Questions

Direction

- Should I exclude the gyroscopic-based stabilization?
- Eigen values of linearized system, Poincare map analysis, anything else I should study for the stability analysis?
- The linkage between the control in simulation and mechanism design
  - Parameters
  - How to design a mechanism can emulate PD control?

General Utilities

- Any solver for nonlinear program IHMC used?
- Any trajectory optimization package IHMC used?
- Methods to get stable Reciprocating Spoked Runner?

Past simulations

- Why the abstract runner (in spoked runner project) can be stabilized in x direction?

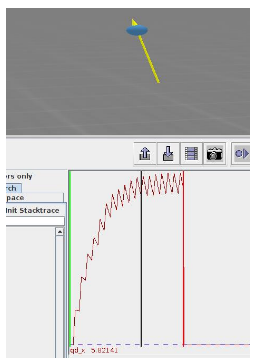

Figure 1: The Abstract Runner

  - The simulation setup is really robust for a large set of initial conditions/throttle angles
  - It turns out its because the added wind resistance dissipate a lot of energies.

- Methods to get stable Reciprocating Spoked Runner?
- What is the line private static final long serialVersionUID for?

2 Pitch Stability of an Vertically Open-loop Hopper

2.1 Jorge Cham's Dissertation - openloop control of 1DOF vertical hopper

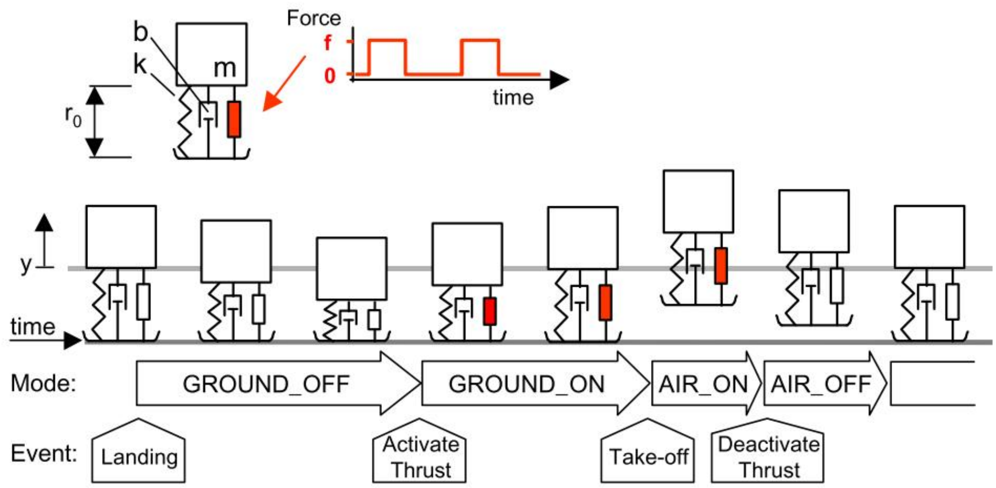

Figure 3-1. The vertical hopping model used for analysis. The hopper's leg consists of a spring, a damper and a force element which is active according to a binary motor pattern. The figure shows a sample trajectory of the hopper, the different modes that it goes through, and the events that trigger the transitions between the modes.

Figure 2: The schematic of a 1 DOF hopper [11]

2.1.1 Equation of motion

Using the model as shown in Fig. 2, during the stand phase (i.e. $y \leq 0$), the equation of motion can be expressed as:

$$m\ddot{y} = -b\dot{y} + -ky - mg + f$$

where m is the mass, b is the damping, k is the stiffness, f is the control input. Normalized by weight, the equation becomes

$$\ddot{y} = -b/m\dot{y} + -k/my - g + f/m$$

Expressed in state space form:

$$\begin{bmatrix} \dot{y} \\ \ddot{y} \end{bmatrix} = \begin{bmatrix} 0 & 1 \\ -k/m & -b/m \end{bmatrix} \begin{bmatrix} y \\ \dot{y} \end{bmatrix} + \begin{bmatrix} 0 \\ -g + f/m \end{bmatrix} \tag{1}$$

or equivalently

$$\dot{X} = \begin{bmatrix} 0 & 1 \\ -\omega^2 & -2\xi\omega \end{bmatrix} X + \begin{bmatrix} 0 \\ -g + f_n(t) \end{bmatrix} = \begin{bmatrix} 0 & 1 \\ -k_p & -k_d \end{bmatrix} X + \begin{bmatrix} 0 \\ -g + f_n(t) \end{bmatrix} \tag{2}$$

where $X \triangleq [y, \dot{y}]^T$. When the hopper is in the air (i.e. $y > 0$, flight phase),

$$\dot{X} = \begin{bmatrix} 0 & 1 \\ 0 & 0 \end{bmatrix} X + \begin{bmatrix} 0 \\ -g \end{bmatrix} \tag{3}$$

Define the force of an open-loop motor pattern

$$f_n(t) = \begin{cases} f/m, & \text{if } t_{off} < t < t_{off} + t_{on}. \\ 0, & \text{otherwise.} \end{cases} \tag{4}$$

2.2 Stability Analysis of an Open-loop Controlled Hopper with Discrete Pitch Angle Control

Use the state space of z motion form 2 with a simplified open-loop force input:

$$\begin{bmatrix} \dot{z} \\ \ddot{z} \end{bmatrix} = \begin{bmatrix} 0 & 1 \\ -kp_z & -kd_z \end{bmatrix} \begin{bmatrix} z \\ \dot{z} \end{bmatrix} + \begin{bmatrix} 0 \\ -g + f_n(t) \end{bmatrix} \tag{5}$$

where

$$f_n(t) = \begin{cases} f_n \triangleq f/m, & \text{if } t_{flight} < t < t_{flight} + t_{contact}. \\ 0, & \text{otherwise.} \end{cases} \tag{6}$$

To further simplify the problem, assuming $f_n(t)$ is much more dominant than $-kp_z z - kd_z \dot{z}$-g so that:

$$\begin{bmatrix} \dot{z} \\ \ddot{z} \end{bmatrix} \approx \begin{bmatrix} 0 & 1 \\ 0 & 0 \end{bmatrix} \begin{bmatrix} z \\ \dot{z} \end{bmatrix} + \begin{bmatrix} 0 \\ f_n(t) \end{bmatrix} \tag{7}$$

Assumptions:

- $f_n(t)$[1] can induce stable vertical hopping motion.
- t_0 starts when the foot leaves the ground.
- $t_{flight} + t_{contact} = T$, $t_{contact} = \alpha$, and $T > \alpha$

Then the pitch dynamics with feedback control can be expressed as:

$$\begin{bmatrix} \dot{\theta} \\ \ddot{\theta} \end{bmatrix} = \begin{bmatrix} 0 & 1 \\ 0 & 0 \end{bmatrix} \begin{bmatrix} \theta \\ \dot{\theta} \end{bmatrix} + \begin{bmatrix} 0 \\ -f_n(t)m/I\Delta x \end{bmatrix} \tag{8}$$

2.2.1 Poincare Section

Denote the state at the n^{th} step Poincare section $\theta_n, \dot{\theta}_n$ (defined at the start of the flight phase). Then we can calculate the state at Poincare section at the $n+1^{th}$ step:

$$\begin{aligned} \dot{\theta}_{n+1} &= \dot{\theta}_n - \frac{f}{I}\Delta x t_{contact} \qquad (9) \\ \theta_{n_{touchDown}} &= \theta_n + \dot{\theta}_n t_{flight} \\ \dot{\theta}_{n_{touchDown}} &= \dot{\theta}_n \\ \theta_{n+1} &= \theta_n + \dot{\theta}_n t_{flight} + \dot{\theta}_n t_{contact} - \frac{1}{2}\frac{f}{I}\Delta x t_{contact}^2 \\ &= \theta_n + T\dot{\theta}_n - \frac{1}{2}\frac{f}{I}\alpha^2 \Delta x \qquad (10) \end{aligned}$$

2.2.2 Poincare Map of Pitch Dynamics with Proportional Control

By designing a proportional control such that $\Delta x = k\phi_n$ and defining $K = \frac{1}{2}\frac{f}{I}k$, Eq. 9 and Eq.10 can be expressed as follows:

$$\begin{aligned} \theta_{n+1} &= \theta_n - \alpha^2 K \theta_n + T\dot{\theta}_n \\ \dot{\theta}_{n+1} &= \dot{\theta}_n - 2\alpha K \theta_n \end{aligned}$$

[1]Conceptually, the $f_n(t)$ can be treated as a force applied from a nonlinear component which connects the massless leg to the body (so there is no velocity change happen at foot strike)

Arranged them in the state space equation, we can get a discrete map M (i.e. Poincare Map, with set of difference equations):

$$\begin{bmatrix}\theta_{n+1}\\ \dot{\theta}_{n+1}\end{bmatrix} = \begin{bmatrix}1-\alpha^2 K & T\\ -2\alpha K & 1\end{bmatrix}\begin{bmatrix}\theta_n\\ \dot{\theta}_n\end{bmatrix} = M\begin{bmatrix}\theta_n\\ \dot{\theta}_n\end{bmatrix} \tag{11}$$

Eigen value analysis
To analyze the stability of the equation in 11, we need to check whether the eigen values of Poincare map M are within the unit cycle. Similar to the Rooth-Herwitz method for the continuous map, we can use Jury Stability Test (Ogata, 1985)[2], which states that a discrete system of two dimensions with the characteristic equations P(z) of the form:

$$P(z) = a_0 z^2 + a_1 z + a_2$$

where $a_0 > 0$, is stable if the following conditions are all satisfied:

$$\begin{aligned} |a_2| &< a_0 \\ a_0 + a_1 + a_2 &> 0 \\ a_0 - a_1 + a_2 &> 0 \\ |(a_0 + a_2)(a_2 - a_0)| &> |a_1(a_0 - a_1)| \end{aligned}$$

For a Jacobian of the form

$$J = \begin{bmatrix} J_1 & J_2 \\ J_3 & J_4 \end{bmatrix}$$

The characteristics equation can be expressed as follows:

$$P(z) = z^2 - (J_1 + J_4)z + (J_1 J_4 - J_2 J_3)$$

Substituting into the stable conditions stated above,

$$|(J_1 J_4 - J_2 J_3)| < 1 \tag{12}$$
$$1 - (J_1 + J_4) + (J_1 J_4 - J_2 J_3) > 0 \tag{13}$$
$$1 + (J_1 + J_4) + (J_1 J_4 - J_2 J_3) > 0 \tag{14}$$
$$|(1 + (J_1 J_4 - J_2 J_3))((J_1 J_4 - J_2 J_3) - 1)| > |(J_1 + J_4)(1 + (J_1 + J_4)| \tag{15}$$

Check condition Eq.12:
First assuming $1 - \alpha^2 K + 2T\alpha K > 0$

$$\begin{aligned} 1 - \alpha^2 K + 2T\alpha K &< 1 \\ \rightarrow -\alpha^2 K + 2T\alpha K &< 0 \\ \rightarrow \alpha K(-\alpha + 2T) &< 0 \end{aligned}$$

Since $\alpha > 0$, $K > 0$, and $T > \alpha$, the assumption cannot satisfy the condition.
Next, assuming $1 - \alpha^2 K + 2T\alpha K < 0$:

$$\begin{aligned} 1 - \alpha^2 K + 2T\alpha K &> -1 \\ \rightarrow -1 + \alpha^2 K - 2T\alpha K &< 1 \\ \rightarrow \alpha K(\alpha - 2T) &< 2 \end{aligned}$$

Since $T > \alpha$, the condition can always be satisfied, as long as the following condition is satisfied:

$$(J_1 J_4 - J_2 J_3) = (1 - \alpha^2 K + 2T\alpha K) < 0$$

[2]contents quotated from [11]

Combine conditions above we can get a new inequality as follows:

$$-1 < (J_1J_4 - J_2J_3) = (1 - \alpha^2K + 2T\alpha K) < 0 \tag{16}$$

Check condition Eq.13:

$$\begin{aligned} 1 - (1 - \alpha^2K + 1) + (1 - \alpha^2K + 2T\alpha K) > 0 \\ \rightarrow 2T\alpha K > 0 \end{aligned}$$

From the last inequality we can get the condition is always hold.

Check condition Eq.14:

$$\begin{aligned} 1 + (1 - \alpha^2K + 1) + (1 - \alpha^2K + 2T\alpha K) > 0 \\ \rightarrow 4 - 2\alpha^2K + 2T\alpha K > 0 \\ \rightarrow 4 + \alpha K(-2\alpha + 2T) > 0 \end{aligned}$$

From the last inequality we can get the condition is always hold.

Check condition Eq.15:
Based on Eq. 16, the left hand side of Eq. 15 can be rearranged as :

$$|(det(M) + 1)(det(M) - 1)| = |det(M)^2 - 1| = 1 - det(M)^2$$

From Eq. 13 and 14 we can got $(J_1 + J_4) > 0$, therefore the right hand side of Eq. 15 can be rearranged as:

$$|(J_1 + J_4)(J_1 + J_4 + 1)| = (J_1 + J_4)(J_1 + J_4 + 1)$$

Therefore the Eq. 15 can be expressed as follows:

$$1 - det(M)^2 > tr(M)(tr(M) + 1)$$

where $det(M) = \prod_i \lambda_i = (J_1J_4 - J_2J_3)$ is the determinant of matrix M and $tr(M) = \sum_i \lambda_i = (J_1 + J_4)$ is the trace of the matrix M.

To sum up
For the (Poincare) stability, the following conditions need to be satisfied:

$$-1 < det(M) < 0 \tag{17}$$

$$0 < tr(M)(tr(M) + 1) < 1 - det(M)^2 \tag{18}$$

where

$$\begin{aligned} det(M) &= 1 - \alpha^2K + 2T\alpha K \\ tr(M) &= 2 - \alpha^2K \\ K &= \frac{1}{2}\frac{f_n}{I}k \end{aligned}$$

Result
After check the sign of the $det(M)$, it was found that $det(M)$ always > 0:

$$1 - \alpha^2K + 2T\alpha K = 1 + \alpha K(-\alpha + 2T) > 0$$

Therefore, it is concluded that proportional control with this system setup cannot stablize the pitch dynamics.

2.2.3 Poincare Map of Pitch Dynamics with PD Control

By designing a PD control such that $\Delta x = k_p\theta_n + k_d\dot{\theta}_n$ and defining $K = \frac{1}{2}\frac{f}{I}k_p$, $C = \frac{1}{2}\frac{f}{I}k_d$, Eq. 9 and Eq.10 can be expressed as follows:

$$\begin{aligned}
\theta_{n+1} &= \theta_n - \alpha^2 K\theta_n + T\dot{\theta}_n - \alpha^2 C\dot{\theta}_n \\
\dot{\theta}_{n+1} &= \dot{\theta}_n - 2\alpha K\theta_n - 2\alpha C\dot{\theta}_n
\end{aligned}$$

Arranged them in the state space equation, we can get a discrete map M_{pd}:

$$\begin{bmatrix}\theta_{n+1} \\ \dot{\theta}_{n+1}\end{bmatrix} = \begin{bmatrix}1-\alpha^2 K & T-\alpha^2 C \\ -2\alpha K & 1-2\alpha C\end{bmatrix}\begin{bmatrix}\theta_n \\ \dot{\theta}_n\end{bmatrix} = M_{pd}\begin{bmatrix}\theta_n \\ \dot{\theta}_n\end{bmatrix} \tag{19}$$

2.2.4 Analytical Solution for Eq.7

Start from t_0 (the beginning of the flight phase), assuming $Z = [0, \dot{z}_0]^T$, then we can get:

$$z(t_{flight}) = \dot{z}_0 t_{flight} - 1/2 g t_{flight}^2 = 0 \tag{20}$$
$$\dot{z}(t_{flight}) = \dot{z}_0 - g t_{flight} = -\dot{z}_0 \tag{21}$$

where a constraint for the $\dot{z}_0$ can be derived:

$$\dot{z}_0 = 1/2 g t_{flight} \tag{22}$$
$$\tag{23}$$

Then we can derive the solution at the end of the touch down:

$$z(1) = -\dot{z}_0 t_{contact} + (f/m - g) t_{contact}^2 = 0 \tag{24}$$
$$\dot{z}(1) = -\dot{z}_0 + (f/m - g) t_{contact} = \dot{z}_0 \tag{25}$$

where another constraint for the $\dot{z}_0$ can be derived:

$$\dot{z}_0 = 1/2(f/m - g) t_{contact} \tag{26}$$

Period T, contact force f and $t_{contact}$ are dependent From Eqs. 26 and 22 we can get

$$\begin{aligned} 1/2 g t_{flight} &= 1/2(f/m - g) t_{contact} \\ \rightarrow t_{flight} &= (f/mg - 1) t_{contact} \\ \rightarrow t_{flight} + t_{contact} = T &= (f/mg) t_{contact} \end{aligned}$$

2.3 Stability Analysis of an Open-loop Controlled Hopper with Continuous Pitch Angle Control

Consider the case that $\Delta x = k\theta(t)$ or $\Delta x = k_p\theta(t) + k_d\dot{\theta}(t)$, then the pitch angle will be controlled continuously in the stance phase. The flight phase remained the same as there is no ground reaction force can act on the body:

$$\dot{X} = \begin{bmatrix} \dot{\theta} \\ \ddot{\theta} \end{bmatrix} = \begin{bmatrix} 0 & 1 \\ 0 & 0 \end{bmatrix} \begin{bmatrix} \theta \\ \dot{\theta} \end{bmatrix} \tag{27}$$

2.3.1 Poincare map of Hopper with Continuous Proportional Control

Assuming $\Delta x = k\theta(t)$, then the system dynamic in the stance phase becomes:

$$\dot{X} = \begin{bmatrix} \dot{\theta} \\ \ddot{\theta} \end{bmatrix} = \begin{bmatrix} 0 & 1 \\ -k\frac{f}{I} & 0 \end{bmatrix} X \triangleq \begin{bmatrix} 0 & 1 \\ -2K & 0 \end{bmatrix} X = AX \tag{28}$$

where $K = \frac{1}{2}\frac{f}{I}k$. Again denoting the state at the n^{th} step Poincare section $\theta_n, \dot{\theta}_n$ (defined at the start of the flight phase). Then we can first calculate the touchdown state at n_{th} step:

$$\begin{aligned} \theta_{n_{TD}} &= \theta_n + \dot{\theta}_n t_{flight} \\ \dot{\theta}_{n_{TD}} &= \dot{\theta}_n \end{aligned}$$

Next, assuming the contact time is exactly $t_{contact} = \alpha$ (e.g. no perturbation in z direction), then the $X_{n+1} = [\theta_{n+1}, \dot{\theta}_{n+1}]^T$ can be expressed with $X_{n_{TD}} = [\theta_{n_{TD}}, \dot{\theta}_{n_{TD}}]^T$:

$$\begin{aligned} X_{n+1} &= e^{A\alpha}(X_{nTD} - X_{eq}) + X_{eq} & (29) \\ &= e^{A\alpha}(\begin{bmatrix} 1 & (T-\alpha) \\ 0 & 1 \end{bmatrix} (X_n - X_{eq}) + X_{eq} & (30) \end{aligned}$$

where $X_{eq} = [0, 0]^T$ is the equilibrium point of Eq. 28. Therefore, we can get the Poincare map in this case is:

$$\begin{aligned} M &= e^{A\alpha}(\begin{bmatrix} 1 & (T-\alpha) \\ 0 & 1 \end{bmatrix} & (31) \\ &= \begin{bmatrix} 1 & T-\alpha+e^{\alpha} \\ e^{-2K\alpha} & e^{-2K\alpha}(T-\alpha)+1 \end{bmatrix} & (32) \end{aligned}$$

2.3.2 Poincare map of Hopper with Continuous PD Control

Assuming $\Delta x = k_p\theta(t) + k_d\dot{\theta}(t)$, then the system dynamic in the stance phase becomes:

$$\dot{X} = \begin{bmatrix} \dot{\theta} \\ \ddot{\theta} \end{bmatrix} = \begin{bmatrix} 0 & 1 \\ -k_p\frac{f}{I} & -k_d\frac{f}{I} \end{bmatrix} X \triangleq \begin{bmatrix} 0 & 1 \\ -2K & -2C \end{bmatrix} X = AX \tag{33}$$

Therefore, we can get the Poincare map in this case is:

$$\begin{aligned} M &= e^{A\alpha}(\begin{bmatrix} 1 & (T-\alpha) \\ 0 & 1 \end{bmatrix} & (34) \\ &= \begin{bmatrix} 1 & T-\alpha+e^{\alpha} \\ e^{-2K\alpha} & e^{-2K\alpha}(T-\alpha)+e^{-2C\alpha} \end{bmatrix} & (35) \end{aligned}$$

2.3.3 General Solution of Poincare map of Hybrid Linear Systems

$$\dot{Z} = AZ + B \tag{36}$$

where **A is invertible**. If the **mode transistion is time-based**, then we can augment the state of the system with t:

$$\dot{X} = \begin{bmatrix} \dot{t} \\ \dot{Z} \end{bmatrix} = \begin{bmatrix} 0 & 0 \\ 0 & A \end{bmatrix} X + \begin{bmatrix} 1 \\ B \end{bmatrix} \tag{37}$$

where $X = [t, Z]^T$. Assuming the mode trasition happened under the following condition:

$$e^T X = 0 \tag{38}$$

and takes time Δt from X_n to X_{n+1}, then the Poincare map (Jacobian matrix) can be expressed as:

$$\frac{\partial X_{n+1}}{\partial X_n} = -\dot{X}_{n+1}(e^T \dot{X}_{n+1})^{-1} e^T \begin{bmatrix} 1 & 0 \\ 0 & e^{A\Delta t} \end{bmatrix} + \begin{bmatrix} 1 & 0 \\ 0 & e^{A\Delta t} \end{bmatrix} \tag{39}$$

3 Simulations

3.1 1 DOF Vertical Hopper with Open-loop Control[11]

System Setup

- Body mass $m = 1$ kg with massless leg, $l = 1$ m.
- Spring parameters: $\omega_n = 30$ rad/s, $\xi = 0.15$ (or equivalently, $kp = 900, kd = 9$)
- Static initial condition, COM height $= 1.3$ m (foot to ground $= 0.3$ m)
- Open-loop external force:

$$f_n(t) = \begin{cases} f_n \in \mathbb{C}, & \text{if } t \in t_{on}. \\ 0, & \text{otherwise.} \end{cases}$$

- t_{on}: The duration of actuator activation, starts when the spring reaches the maximum compression, ends when the contact point leave the ground.

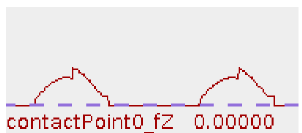

Figure 3: Ground reaction force when $f_n = 10$ N

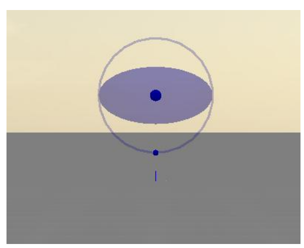

Figure 4: The vertical hopper, the blue dot at the bottom is the contact point of the massless leg.

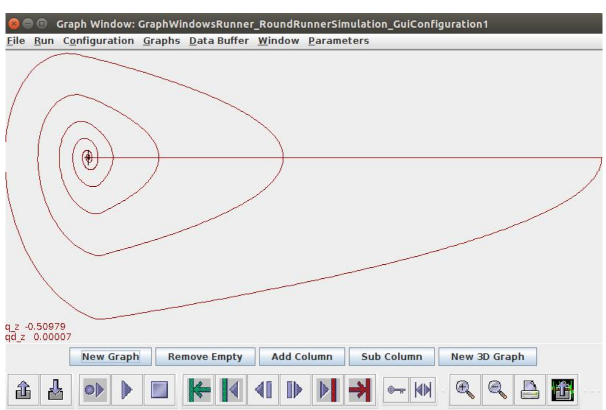

Figure 5: Phase portrait (stable spiral) of $f = 1$ N, period 0 sec

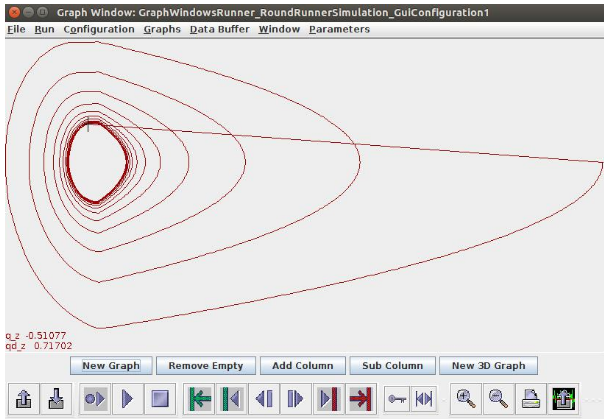

Figure 6: Phase portrait (stable limit cycle) of $f = 10$ N, period 0.27sec, (closer to the damped natural period $\approxeq 0.3295$ sec)

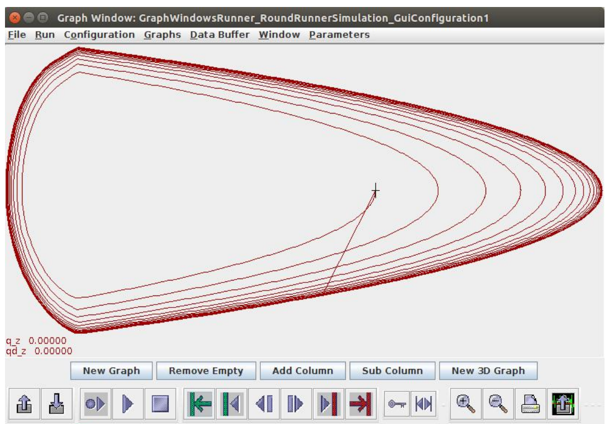

Figure 7: Phase portrait (stable limit cycle) of $f = 50$ N, period 0.859 sec

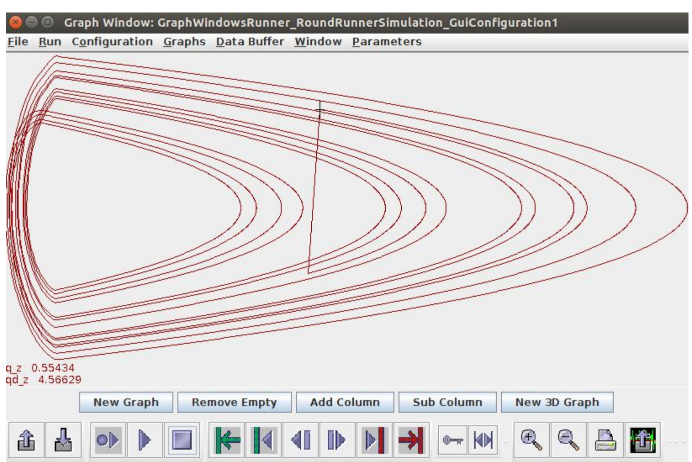

Figure 8: Phase portrait of $f = 100$ N, no stable limit cycle evolved (might be bifurcation).

Plan

- Go through and reuse the Poincare analysis in spokedRunner package.

- Could be a good case for me to learn how to use parameterOptimizer (or other constrained nonlienar program solver) to get IC/parameters for a stable/optimal gait.

3.2 Abstract Runner with Open-loop Normal Force and Closed-loop Pitch Angle Control

System Setup

- Body mass $m = 10$, $I_{yy} = 10$ with massless leg, $l = 1$.
- Reuse the vertical hopper above, change the initial condition to $\theta = 0.2$
- No force applied in the x direction, $\dot{x}_0$ can be 0 (hopper) or a constant (runner).
- Similar to the abstract runner (Fig. 9), enforces the on/off timing of ground reaction force $f_n(t)$:

$$f_n(t) = \begin{cases} (f_n + u) | f_n \in \mathbb{C}, & \text{if } t \in t_{on}. \\ 0, & \text{otherwise.} \end{cases}$$

where $f_n = \alpha * mg$, $\alpha \in \mathbb{C}$, u is the force from PD control, $kp_z = 80, kd_z = 6$. $kp_{pitch} = 80, kd_{pitch} = 6$

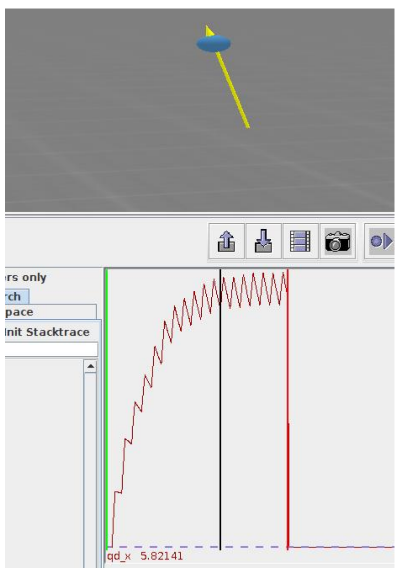

Figure 9: The Abstract Runner

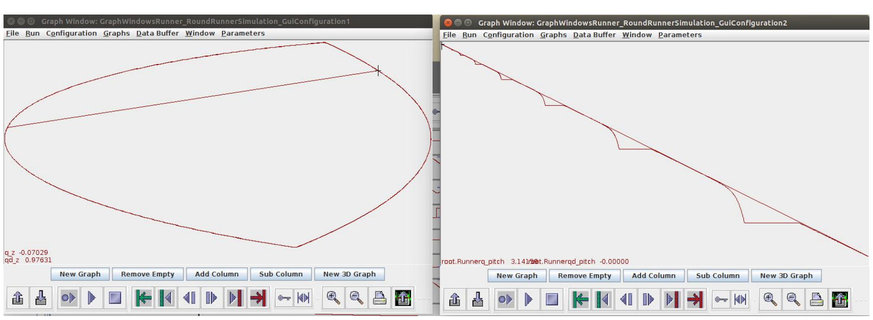

Figure 10: The phase portrait of the abstract runner: phase portrait (left) of body z movement $[q\_z, qd\_z]^T$ and the pitch motion (right, the movement is converging to the origin in the upper-left corner) .

Plan

- Link it to the Math from Jerry's note (analysis of a linear Poincare map) to get the boundaries of stable parameters.

3.3 Spoked Runner with Massless Legs

System Setup

- $m = 15$, $I_{yy} = 10$, $l = 4$, $r_{penetration} = 0.3$ (the distance the virtual wheel penetrate into the ground)
- Adjustable spoke leg number
- Fixed rotation rate w.r.t inertial frame
- Setup of contact force: PD control
  - w.r.t to world frame
  - w.r.t to inertial frame (virtual pivot point)
- Assuming no friction (Could be an bad idea?)

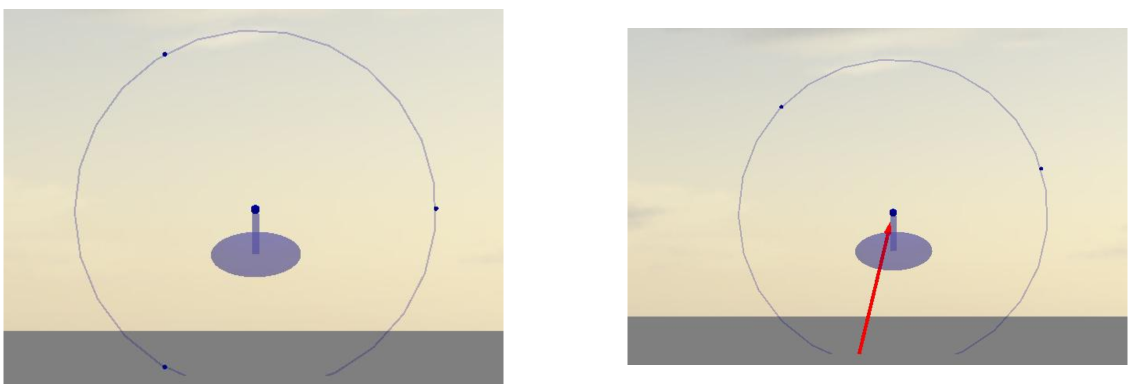

Figure 11: The Spoked Runner with three legs

Plan

- Smoothly change the leg length, or the rotational speed of the virtual wheel, and observe the system response.
- Learn how to use GUI for parameter adjustment with SCS.

4 Code implementation

4.1 Modeling and Parameters

Main idea: a virtual wheel (as the massless leg) with radius r_{wheel} penetrate the ground for a distance r_{pen} where a external force point pe is attached on it. A body (with mass m and inertia Iyy) is attached to the center of wheel. Using PD control to interpret contact force when p_e is under the ground.

06/07 First prototype (Not used now)

- Joint numbers: 2
- Joint types: Floating planer joint for virtual wheel and pin joint for the body link.
- Contact point type: External force point
- Virtual wheel rotation: set proper initial condition for virtual wheel (also need a large inertia to make it nearly constant).

Contact force: Assuming the ground height is 0,

$$F_z = kp(0 - pe_z) + kd(0 - ve_z) \tag{40}$$
$$\phi = atan2(pe_x, r_{wheel} - pe_z) \tag{41}$$
$$F_x = F_z tan(\phi) \tag{42}$$

where ve is the velocity vector of the contact point pe, kp and kd are the PD control parameters. F_x is calculated so that the vector of ground reaction force $[F_x, F_y, F_z]^T$ will point towards the virtual pivot (the center of the virtual wheel).

Assessments:

- Need to set a non-zero inertia of massless virtual wheel (for numerical stability), otherwise the simulation will diverge.
- The inertia of virtual wheel need to be a large one for constant rotational speed.
- Suggestions: remove the massless link, attach the external force point to the body and change its position in the controller every time step.

06/08 Round Runner

- Joint numbers: 1
- Joint types: Floating planer joint for the body link.
- Contact point type: External force point
- Virtual wheel rotation: Assigning the external force point location with respect to the joint in an open loop manner.
- Contact force: Assuming the ground height is 0,

$$F_z = kp(0 - pe_z) + kd(0 - ve_z) \tag{43}$$
$$\phi = atan2(pe_x, r_{wheel} - pe_z) \tag{44}$$
$$F_x = F_z tan(\phi) \tag{45}$$

  where ve is the velocity vector of the contact point pe, kp and kd are the PD control parameters. F_x is calculated so that the vector of ground reaction force $[F_x, F_y, F_z]^T$ will point towards the virtual pivot (the center of the virtual wheel).

Assessments:

- The ground reaction force looks better, while the energy is not balanced (after a while it will move towards the negative x direction)
- The inertia of virtual wheel need to be a large one for constant rotational speed.
- Suggestions: Use the ground contact point (instead of external force point) to see how it goes.

06/11 Round Runner(with Ground Contact Point)

- Joint numbers: 1
- Joint types: Floating planer joint for the body link.
- Contact point type: Ground contact point, linear contact model[1]
- Virtual wheel rotation: Assigning the external force point location with respect to the joint in an open loop manner.
- **Contact point number** Parameterized, currently set to 3-6 points.
- Contact force: using built-in functionalities, only assigning the kp, kd (PD parameters in the z direction), kp_x, and kd_x (PD parameters in the x/y directions).

Assessments:

- Was able to generate a stable walking. Contact point has sliding.
- Due to setting up stiffness and damping for x and z separately, the force is not always point towards the virtual pivot.

06/12 Round Runner(with External Contact Point Point)

- Implement the same one as 06/11, but replace the ground contact point to the external one (because it is more complex for ground contact point to adjust stiffness/damping as parameters.)
- implement the linear ground contact model basically.

06/13 Round Runner

- Parameterize contact point numbers
- Adding enum for switching between different setup: contact point type and the corresponding ground reaction force calculation: (w.r.t to the world frame or inertia frame.)

06/16 Round Runner (vertical hopper)

- Adding vertical hopper with open-loop force control
- Playing with open-loop force magnitudes for different stability conditions

[1] Disable the hardening stiffness in z direction by setting groundStiffeningLength to Double.NEGATIVE_INFINITY

5 Info might be useful

5.1 Going through references

1. Compare different terrestiral locomotions: Some parameters of the walk are not speed- dependent. The swing duration is a constant time parameter [1].
2. Trunk plays an important role during walking (birds) [2].
3. The use of these drives (Resonance drives, with adaptive control) allows increasing machine's quickness several times and decreasing energy expenses simultaneously 10-50 times [3].
4. Light weight leg (ostrich vs. moa) can run faster[5]. Also a famous allometric equation:

$$Y = M^{3/4} \tag{46}$$

   where M is the body mass, Y is the metabolic rate.
5. Human's walking may not be really self-optimized: the preferred speed maybe different from the energetically optimal speed[8].
6. It is concluded that the most important adjustment to the bodys spring system to accommodate higher stride frequencies is that leg spring becomes stiffer [19].
7. magic equations for imd force (ostrich) [26]
8. gait frequency was reported to be highly correlated with the resonant frequency of the mass-spring model [30]
9. WABIAN, why you are here? [31]

5.2 Categories

1. Nonlinear oscillators/components [3, 6, 9, 10, 12, 28, 39];
2. zoology, biomechanics of animals: [1, 2, 4, 5, 16]
3. Bio-inspired robots: [7, 32]
4. Reference I should read: [11, 15, 27, 28]
5. Article not found (or not free)[4].
6. Robots in 3D: [13]
7. Stability analysis (Monocycle, linearized system) [14] (Limit cycle) [11, 27] dimensionless [41]
8. Biology/Anatomical structure [17, 20]
9. Light weight fast robot [18, 25]
10. take a look again [21]
11. mechanism design of robot [22]
12. quadruped reference [23] MIT Cheetah[37]
13. human energy cost, resonance usage [24, 8, 38, 40]
14. walking parameterization [29, 21, 42]
15. human-animal differences [15]
16. open-loop robot [33], passive robot [35, 34, 36]

References

[1] Anick Abourachid. Kinematic parameters of terrestrial locomotion in cursorial (ratites), swimming (ducks), and striding birds (quail and guinea fowl). *Comparative Biochemistry and Physiology Part A: Molecular and Integrative Physiology*, 131(1):113–119, dec 2001.

[2] Anick Abourachid, Remi Hackert, Marc Herbin, Paul A. Libourel, François Lambert, Henri Gioanni, Pauline Provini, Pierre Blazevic, and Vincent Hugel. Bird terrestrial locomotion as revealed by 3D kinematics. *Zoology*, 114(6):360–368, dec 2011.

[3] T. Akinfiev and M. Armada. Elements of built-in diagnostics for resonance drive with adaptive control system. In *International Symposium on Automation and Robotics in Construction*, pages 617–621, Madrid, Spain, 1999.

[4] R. Mc N Alexander, G. M O Maloiy, R. Njau, and A. S. Jayes. Mechanics of running of the ostrich (Struthio camelus). *Journal of Zoology*, 187(2):169–178, 1979.

[5] R. McNeill Alexander. The legs of ostriches (Struthio) and moas (Pachyornis). *Acta Biotheoretica*, 34(2-4):165–174, 1985.

[6] G. V. Anand. Nonlinear Resonance in Stretched Strings with Viscous Damping. *The Journal of the Acoustical Society of America*, 40(6):1517–1528, 1966.

[7] Arvind Ananthanarayanan, Mojtaba Azadi, and Sangbae Kim. Towards a bio-inspired leg design for high-speed running. *Bioinspiration and Biomimetics*, 7(4):046005, dec 2012.

[8] Elizabeth Arnall, Jessica Pyatt, Chelsie Rice, Katie L Anderson, and Duncan Mitchell. Resonance in Human Walking Economy: How Natural Is It? *International Journal of Undergraduate Research and Creative Activities*, 4(1), 2012.

[9] V. I. Babitsky and M. Y. Chitayev. Adaptive high-speed resonant robot. *Mechatronics*, 6(8):897–913, dec 1996.

[10] Jonas Buchli, Fumiya Iida, and Auke Jan Ijspeert. Finding resonance: Adaptive frequency oscillators for dynamic legged locomotion. In *IEEE International Conference on Intelligent Robots and Systems*, pages 3903–3909, Beijing, China, 2006.

[11] J. G. Cham. *On Performance and Stability in Open-Loop Running*. PhD thesis, Stanford University, 2002.

[12] S. Chatterjee and Anindya Malas. On the stiffness-switching methods for generating self-excited oscillations in simple mechanical systems. *Journal of Sound and Vibration*, 331(8):1742–1748, apr 2012.

[13] Michael J. Coleman, Anindya Chatterjee, and Andy Ruina. Motions of a rimless spoked wheel: a simple three-dimensional system with impacts. *Dynamics and Stability of Systems*, 12(3):139–159, 1997.

[14] Michael J. Coleman and Jim M. Papadopoulos. Intrinsic stability of a classical monocycle and a generalized monocycle. In *Bicycle and Motorcycle Dynamics, Symposium on Dynamics and Control of Single Track Vehicles*, Delft, Netherlands, 2010.

[15] M. A. Daley and A. A. Biewener. Running over rough terrain reveals limb control for intrinsic stability. *Proceedings of the National Academy of Sciences*, 103(42):15681–15686, oct 2006.

[16] M. A. Daley, G. Felix, and A. A. Biewener. Running stability is enhanced by a proximo-distal gradient in joint neuromechanical control. *Journal of Experimental Biology*, 210(3):383–394, feb 2007.

[17] T. El-Mahdy, S. M. El-Nahla, L. C. Abbott, and S. A.M. Hassan. Innervation of the pelvic limb of the adult ostrich (Struthio camelus). *Journal of Veterinary Medicine Series C: Anatomia Histologia Embryologia*, 39(5):411–425, 2010.

[18] Darrell Ethington. Dash Robotics Reveals A DIY High-Speed Running Robot Kit, Which Hobbyists Can Own For Just $65, 2013.

[19] Claire T. Farley and Octavio González. Leg stiffness and stride frequency in human running. *Journal of Biomechanics*, 29(2):181–186, 1996.

[20] D. Gangl, G. E. Weissengruber, M. Egerbacher, and G. Forstenpointner. Anatomical description of the muscles of the pelvic limb in the ostrich (Struthio camelus). *Journal of Veterinary Medicine Series C: Anatomia Histologia Embryologia*, 33(2):100–114, 2004.

[21] S. M. Gatesy and A. A. Biewener. Bipedal locomotion: effects of speed, size and limb posture in birds and humans. *Journal of Zoology*, 224(1):127–147, 1991.

[22] Martin Grimmer and André Seyfarth. Design of a Series Elastic Actuator driven ankle prosthesis : The trade-off between energy and peak power optimization. In *Dynamic Walking*, 2011.

[23] R Hackert, H Witte, and M S Fischer. Interactions between motions of the trunk and the angle of attack of the forelimbs in synchronous gaits of the pika (Ochotona rufescens). In *Adaptive Motion of Animals and Machines*, pages 69–77. Springer, 2006.

[24] Kenneth G. Holt, Joseph Hamill, and Robert O. Andres. Predicting the minimal energy costs of human walking. *Medicine & Science in Sports & Exercise*, 23(4):491–498, 1991.

[25] Fumiya Iida, Murat Reis, Nandan Maheshwari, Xiaoxiang Yu, and Amir Jafari. Toward efficient, fast, and versatile running robots based on free vibration. In *Dynamic Walking*, Pensacola, FL, 2012.

[26] D. L. Jindrich, N. C. Smith, K. Jespers, and A. M. Wilson. Mechanics of cutting maneuvers by ostriches (Struthio camelus). *Journal of Experimental Biology*, 210(8):1378–1390, 2007.

[27] Takahiro Kagawa and Yoji Uno. Necessary condition for forward progression in ballistic walking. *Human Movement Science*, 29(6):964–976, dec 2010.

[28] Jg Daniël Karssen and Martijn Wisse. Running with improved disturbance rejection by using non-linear leg springs. *International Journal of Robotics Research*, 30(13):1585–1595, sep 2011.

[29] Leng Feng Lee and Venkat N. Krovi. Musculoskeletal simulation-based parametric study of optimal gait frequency in biped locomotion. In *International Conference on Biomedical Robotics and Biomechatronics*, pages 354–359, Scottsdale, AZ, 2008.

[30] Myunghyun Lee, Seyoung Kim, and Sukyung Park. Leg stiffness increases with load to achieve resonance-based CoM oscillation. In *Dynamic Walking*, Pittsburgh, PA, 2013.

[31] Hun-ok Lim, Y Ogura, Atsuo Takanishi, and Proc R Soc A. Locomotion pattern generation and mechanisms of a new biped walking machine. *Proceedings of the Royal Society of London A: Mathematical and Physical Sciences*, 464(2089):273–288, 2008.

[32] R. J. Lock, S. C. Burgess, and R. Vaidyanathan. Multi-modal locomotion: From animal to application. *Bioinspiration and Biomimetics*, 9(1), dec 2014.

[33] Katja Mombaur, H Georg Bock, Johannes Schlöder, and Richard Longman. Stable Walking and Running Robots Without Feedback. In *Climbing and Walking Robots*, pages 725–735. 2005.

[34] Dai Owaki, Masatoshi Koyama, Shin'ichi Yamaguchi, Shota Kubo, and Akio Ishiguro. A two-dimensional passive dynamic running biped with knees. In *Proceedings - IEEE International Conference on Robotics and Automation*, pages 5237–5242, 2010.

[35] Dai Owaki, Masatoshi Koyama, Shin'Ichi Yamaguchi, Shota Kubo, and Akio Ishiguro. A 2-D passive-dynamic-running biped with elastic elements. *IEEE Transactions on Robotics*, 27(1):156–162, 2011.

[36] Dai Owaki, Koichi Osuka, and Akio Ishiguro. Understanding the common principle underlying passive dynamic walking and running. *2009 IEEE/RSJ International Conference on Intelligent Robots and Systems, IROS 2009*, pages 3208–3213, 2009.

[37] Hae-won Park, Sangbae Kim, and Our Approach. Variable Speed Galloping Control using Vertical Impulse Modulation for Quadruped Robots : Application to MIT Cheetah Robot Click for Video Overview, 2012.

[38] Sukyung Park. Can human walking be mimicked by resonance-based oscillation? In *The 7th World Congress on Biomimetics, Artificial Muscles and Nano-Bio*, volume 44, page 2013, Jeju Island, South Korea, 2013.

[39] M C Plooij and M Wisse. A spring mechanism for resonant robotic arms. In *Workshop on Human Friendly Robotics*, page 5, 2011.

[40] V. Racic, A. Pavic, and J. M.W. Brownjohn. Experimental identification and analytical modelling of human walking forces: Literature review. *Journal of Sound and Vibration*, 326(1-2):1–49, sep 2009.

[41] Sebastian Riese and Andre Seyfarth. Stance leg control: Variation of leg parameters supports stable hopping. *Bioinspiration and Biomimetics*, 7(1):016006, mar 2012.

[42] Robert E Weems. Locomotor Speeds and Patterns of Running Behavior in Non-Maniraptoriform Theropod Dinosaurs. *New Mexico Museum of Natural History and Science Bulletin*, 37:379–389, 2006.